

High efficiency fully implanted and co-annealed bifacial n-type solar cells

Adeline Lanterne, Samuel Gall, Yannick Veschetti, Raphaël Cabal, Marianne Coig, Frederic Milesi, Aurélie Tauzin

▶ **To cite this version:**

Adeline Lanterne, Samuel Gall, Yannick Veschetti, Raphaël Cabal, Marianne Coig, et al.. High efficiency fully implanted and co-annealed bifacial n-type solar cells. Energy Procedia, 2013, 38, pp.283 - 288. 10.1016/j.egypro.2013.07.279 . cea-02570734

HAL Id: cea-02570734
https://cea.hal.science/cea-02570734

Submitted on 12 May 2020

HAL is a multi-disciplinary open access archive for the deposit and dissemination of scientific research documents, whether they are published or not. The documents may come from teaching and research institutions in France or abroad, or from public or private research centers.

L'archive ouverte pluridisciplinaire **HAL**, est destinée au dépôt et à la diffusion de documents scientifiques de niveau recherche, publiés ou non, émanant des établissements d'enseignement et de recherche français ou étrangers, des laboratoires publics ou privés.

Available online at www.sciencedirect.com

ScienceDirect

Energy Procedia 38 (2013) 283 – 288

Energy Procedia

SiliconPV: March 25-27, 2013, Hamelin, Germany

High efficiency fully implanted and co-annealed bifacial n-type solar cells

Adeline Lanterne[a]*, Samuel Gall[a], Yannick Veschetti[a], Raphaël Cabal[a], Marianne Coig[b], Frédéric Milési[b], Aurélie Tauzin[b]

[a]*CEA- LITEN, INES, 50 av. du Lac Léman, BP332, 73370, Le Bourget du Lac, France*
[b]*CEA- LETI, 17 rue des Martyrs, 38054, Grenoble Cedex 9, France*

Abstract

The aim of the study was to develop a very simple process for the fabrication of large area n-type PERT cells by means of ion implantation. We showed an improvement of the implanted boron activation rate with the annealing temperature by comparing boron SIMS and ECV concentration profiles. A direct positive impact on the boron emitter saturation current density (J_{0e}) was measured. We also investigated the effect of varying the oxidation conditions during the annealing on the implanted boron emitter and the phosphorus BSF quality. Low emitter saturation current density (J_{0e}) of 131 fA/cm^2 was measured on textured surfaces, close to the value obtained with diffused B-emitters. A process flow was developed leading to an average efficiency of 19% on 239 cm^2 bifacial solar cells, using only eight processing steps with two implantations and one activation annealing.

© 2013 The Authors. Published by Elsevier Ltd. Open access under CC BY-NC-ND license.
Selection and/or peer-review under responsibility of the scientific committee of the SiliconPV 2013 conference

Keywords: n-type silicon; boron; phosphorus; ion implantation; high efficiency; co-annealing;

1. Introduction

N-type silicon substrates offer considerable advantages to produce high-efficiency silicon solar cells, as they have no light-induced degradation (LID) effects [1,2] and higher minority carrier lifetimes than p-type silicon wafers, with a lower sensitivity to metallic impurities [3].

Historically, n-type Si substrates were used in photovoltaic industry for advanced technologies as IBC (Interdigitated Back-Contacted cells) manufactured by SunPower or HIT (Heterojunction with Intrinsic Thin-Layer) by Sanyo. More recently 19,5% of efficiency has been obtained in mass production with a

* Corresponding author. Tel.: +33-479-792-057
E-mail address: Adeline.Lanterne@cea.fr

1876-6102 © 2013 The Authors. Published by Elsevier Ltd. Open access under CC BY-NC-ND license.
Selection and/or peer-review under responsibility of the scientific committee of the SiliconPV 2013 conference
doi:10.1016/j.egypro.2013.07.279

simpler process, which corresponds to a bifacial PERT (Passivated Emitter Rear Totally diffused) structure [4]. Two high temperature gaseous diffusions are necessary to manufacture this structure, the first to form the boron (B) front emitter and the second for the phosphorus (P) back surface filed (BSF).

Among the various approaches for reducing the cost ($/W) of these solar cells, the use of ion implantation to create the B emitter and the P BSF is one of the most promising. Many studies [5-6] have shown that this technique not only reduces considerably the number of process steps, but also allows to reach very low emitter saturation current densities (J_{0e}) [7]. A short review of the literature highlights two different ways of processing these implanted n-type PERT solar cells. The first way uses two thermal anneals to activate separately the B implanted emitter and the P implanted BSF and the second way uses a single co-annealing to activate both dopants. The best efficiencies have been obtained thanks to separate anneals [8], due to the challenge to conciliate the high temperature needed to activate the B atoms with an efficient P BSF. But we have chosen to focus our study on the co-annealing process as it could bring a considerable advantage for process industrialization.

The aim of this paper was to develop a very simple process for the fabrication of large-area n-type PERT solar cell. We first investigated the impact of high temperatures annealing on B implanted emitters in order to reach low current saturation densities. During the annealing, an oxidation step allows to create a high quality oxide layer for the passivation. We studied several oxidation conditions and their effects on symmetrically implanted p^+np^+ and n^+nn^+ samples. Bifacial fully implanted n-type solar cells were then fabricated, characterized and compared to the solar cells doped by diffusion.

2. Experimental

Three types of precursor structures were fabricated on 239 cm^2 Cz n-type silicon wafers with resistivity of 3 Ohm.cm: p^+np^+ structures to study the B emitter ; n^+nn^+ structures to study the P BSF ; p^+nn^+ structures to estimate the V_{oc} of the complete solar cell.

Following the wafers texture, p^+ layers were fabricated by B implantation and n^+ layers by P implantation, except for the reference by diffusion where a BCl_3 high temperature gaseous diffusion was used for the p^+ layer and a $POCl_3$ diffusion for the n^+ layer. B and P implantation conditions were fixed in this study, typical B and P implantation doses were between 1E15 and 6E15 at/cm^2 with implantation energies ranging from 5keV to 30keV. The implantation steps were followed by a thermal annealing to activate the dopants (B and/or P depending on the precursor type) including an oxidation step. Both sides were then capped with a SiN_x layer to improve the passivation and for its anti-reflective effect (diffused reference samples were also passivated with a SiO_2/SiN_x stack). Finally an infra-red (IR) firing step was performed to simulate the firing of the screen-printing pastes.

The resistance sheets (R_{sheet}) of the boron emitter were measured using 4-point probe methods. Implied V_{oc} were measured on each sample using QssPC technique before and after the IR firing as well as the J_{0e} on p^+np^+ structure and the J_{0B} (saturation current density of the n^+ BSF) on n^+nn^+ samples.

Complete solar cells were processed on similar 239 cm^2 Cz n-type silicon wafers with resistivity of 3 Ohm.cm. First wafers were randomly textured. B atoms were then implanted on the front side and P on the rear side. A thermal co-annealing with an oxidation step was performed to activate both dopants, followed by SiN_x depositions on the front and rear sides. Grid patterns were screen-printed on each side using an Ag paste on the rear side and an Ag/Al paste on the front side. References with B and P doping made by gaseous diffusions were also processed on 5 Ohm.cm wafers using the same BCl_3 and $POCl_3$ diffusions than on the precursor samples and the same passivation stacks and metallization steps than the implanted cells.

Illuminated (AM1.5) and dark I-V characterization were performed on each solar cell, followed by

SunsVoc and Internal Quantum Efficiency (IQE) measurements.

3. Results and discussion

3.1. High temperature annealing for boron emitter activation

Fig. 1a and Fig. 1b, show the R_{sheet}, J_{0e}, and implied V_{oc} of implanted p^+np^+ samples activated by various thermal anneal schemes. Our experiment was based on a previous study made by H. Boo [9] which shows the improvement of the implied V_{oc} and J_{01} with increasing annealing temperatures and times. To compare our results with this study, we used similar annealing temperatures (950°C, 1000°C and 1050°C) and times (60 min for all the temperatures and 30 min for 1050°C). But we added to these annealings an oxidation step. We confirmed, for our implant conditions, the improvement of the Implied V_{oc} with the temperature and the time, and we measured a similar improvement of the J_{0e}. Contrary to H. Boo's study, the R_{sheet} decreases for increasing temperatures up to 1050°C, no plateau has been reached.

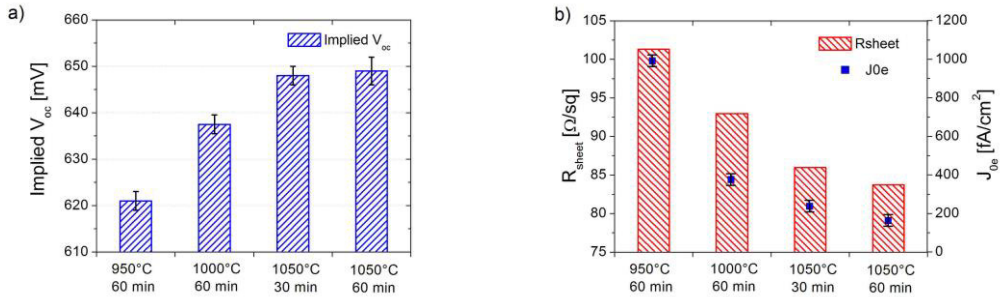


Fig. 1. (a)) Implied V_{oc} measured on B implanted p^+np^+ structures annealed with various conditions; (b) R_{sheet} and J_{0e} measured on the same samples.

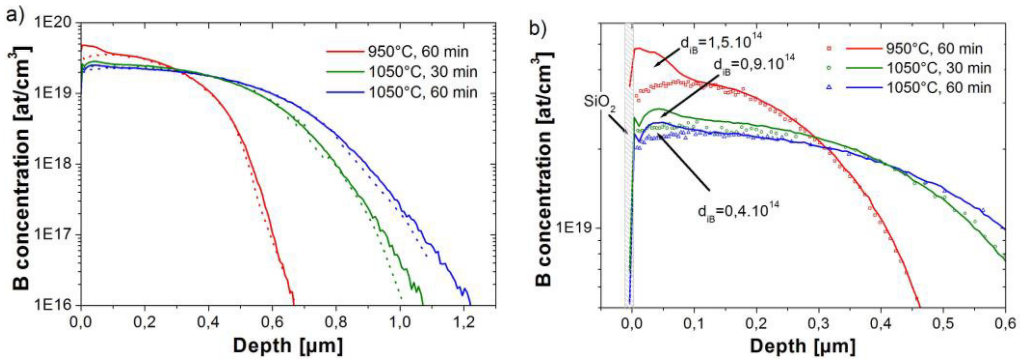


Fig. 2. (a) B concentration profiles measured by SIMS (line) and ECV (dot line) on polished B implanted samples for three annealing conditions; (b) Zoom of Fig. 1a at the surface of the substrate, showing the calculated inactive B dose d_{iB}.

In order to further understand the R_{sheet} decrease, we performed SIMS and ECV (Electrochemical Capacitance Voltage) measurements on B implanted polished wafers annealed with three recipes (950°C 60min, 1050°C 60min and 1050°C 30min with an added oxidation step). The oxide layers were removed before the ECV measurements. The B concentration profiles measured by each technique are shown on

Fig. 2a and 2b. We can observe a large bump in the 950°C SIMS profile near the surface which reduces for higher thermal budget anneals (1050°C anneals) but don't disappear. As these bumps aren't observed on the activated B profiles (ECV profiles), they correspond to inactive B atoms. We quantified this inactive B concentration by integrating both SIMS and ECV profiles and comparing the results. The calculated inactive B doses (d_{iB}) are shown in Fig 2b. A reduction of the d_{iB} is observed by increasing the annealing temperature from 950°C to 1050°C and by increasing the annealing time from 30 min to 60 min at 1050°C. We can conclude that for our implant and annealing conditions, the activation rate increases with the temperature and the time, leading to a reduction of the R_{sheet} as observed on Fig. 1a. The activation rate evolution also explains a part of the improvement of the J_{0e} and the implied V_{oc}, in Fig. 1a and 1b, as both parameters are affected by the recombinations in the emitter.

Table 1. Implied V_{oc} measured on p^+nn^+ implanted samples annealed with various conditions.

Annealing schemes	Implied V_{oc} before IR firing [mV]	Implied V_{oc} after IR firing [mV]
1000°C 30 min + oxidation	620 ± 2	643 ± 4
1000°C 60 min + oxidation	621 ± 4	642 ± 3
1050°C 30 min + oxidation	622 ± 2	642 ± 3
1050°C 60 min + oxidation	621 ± 2	630 ± 4

To measure the impact of these high-thermal budget anneals on implanted P BSF, four anneals with temperatures of 1000°C and 1050°C were performed on p^+nn^+ precursors. After passivations, the implied V_{oc} was measured before and after the IR firing, results are shown on Table 1. The implied V_{oc} is rather constant before IR firing and contrary to p^+np^+ B samples it dramatically drops for the highest thermal budget after the IR firing. This highlights the need to optimize the thermal annealing scheme on p^+nn^+ precursors to associate the high temperatures beneficial for the B emitters and an efficient P BSF.

3.2. Variation of the SiO_2 passivation

After a first optimization of the annealing scheme to maximize the implied V_{oc} of p^+nn^+ structure, several oxidation conditions were tested (from *A* to *C*) on p^+np^+ and n^+nn^+ implanted samples. Fig. 3a and 3b shows the J_{0e}, J_{0B} and implied V_{oc} measured on these samples with reference made by diffusion. J_{0e} and J_{0B}, measured on symmetrically B and P implanted samples respectively, remain constant for the various oxidation conditions with values equal to the diffused samples, as low as 131 fA/cm^2 for the implanted J_{0e}.

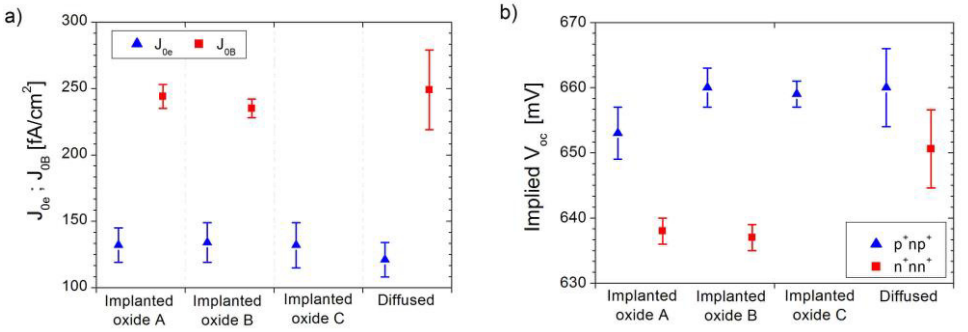


Fig. 3. (a) J_{0e} and J_{0B} measured on symmetrical B and P implanted samples respectively and annealed with various oxidation conditions, compared to diffused BCl_3 and $POCl_3$ samples; (b) Implied V_{oc} measured after IR firing on the same samples.

Even if the oxide conditions variation has no impact on the J_{0e} and J_{0B} values, the oxide *B* and *C* enhance the implied V_{oc} of p^+np^+ samples leading to the same value than BCl_3-diffused samples (660 mV). Concerning the n^+nn^+ samples, lower implied V_{oc} were measured on implanted samples as compared to $POCl_3$-diffused samples, independently of the oxide conditions (oxide *A* or *B*). The oxide *B* condition was chosen for solar cells processing as it allows to reach the highest implied V_{oc} on p^+np^+ samples.

3.3. Solar cells results and characterizations

Several co-annealing schemes were tested for the solar cell processing, only the best anneal condition is shown in Table 2 (average of 5 cells), where it is compared to our previous results and to the diffused solar cells. This co-annealing process provided an average efficiency of 19% which is very close to the best result reported with separated anneals [8] using similar passivation and metallization stacks, and is at the state of the art for a such simple co-annealing process. Compared to our previous study, the optimization of the annealing scheme and of the oxidation conditions, have allowed to improve by 0,5% absolute the solar cells efficiency.

Table 2. Solar cells I-V characterization results.

Process	Voc [mV]	Jsc [mA/cm^2]	FF [%]	η [%]
Optimized Implanted and Co-annealed process	633.6	38.4	78.2	19.0
Previous results [10]	630.7	38.4	76.2	18.5
Diffusion process	637.4	38.6	79.6	19.6

As compared to the diffusion process the implanted solar cells efficiencies are limited by the FF and the V_{oc} even if both parameters have improved since the previous results. The lower implied V_{oc} measured on n^+nn^+ implanted samples on Fig. 3b suggested that the implanted P BSF limits the final V_{oc} of the solar cell. To verify this hypothesis the IQE was measured on diffused and implanted cells. The IQE confirms a better response of the diffused BSF but also shows that the implanted cell has a lower IQE for the short wavelength, so the implanted emitter also affects the V_{oc}.

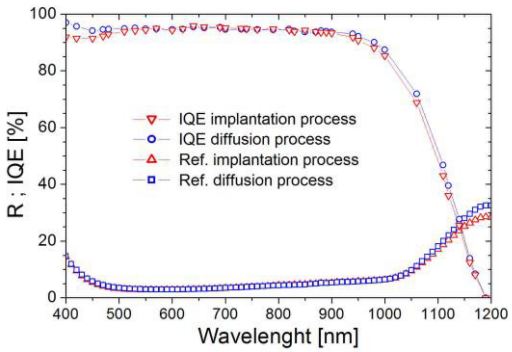


Fig. 4. (a) Internal Quantum Efficiency and Reflectivity measured on diffused and implanted solar cells.

Further characterizations were made to explain the lower FF of the implanted cells. The shunt

resistance (R_{shunt}) and the J_{02} were extracted from the dark-IV curves, PFF was measured by SunsVoc and the series resistance (Rs) were calculated by comparing the SunsVoc and the illuminated-IV curves [11]. The results for the diffused and implanted cells are shown on Table 3.

Table 3. Solar cells characterization: Series resistance, Shunt resistance, PFF and J_{02}.

Process	Rs [Ω.cm^2]	PFF [%]	R_{shunt} [Ω.cm^2]	J_{02} [mA/cm^2]
Optimized Implanted and Co-annealed process	0.41	81.2	12000	1.7E-3
Diffusion process	0.54	83	61000	1E-4

As low Rs are measured on implanted samples they don't impact the FF. However the lower R_{shunt} and the higher J_{02} of implanted cells could both be responsible for lowering the PFF and FF. A laser junction opening was performed on the implanted cells. This opening increases strongly the R_{shunt} which exceeds the diffused value, but only increases the PFF of 0,1% absolute. The J_{02} seems to be the dominating factor that reduced the PFF and FF, its high value has no explanation to date and its origin should be investigated into more details.

4. Conclusion

We showed an improvement of the implanted boron activation rate with the annealing temperature up to 1050°C with a positive influence on the J_{0e}. The necessity of optimizing this annealing with the P BSF was highlighted as well as the positive impact of some oxide conditions. J_{0e} and J_{0b} as low as the diffused emitter and BSF were measured. Our development leaded to an average efficiency of 19% on 239 cm^2 bifacial solar cells, using only 8 processing steps with two implantations and one activation annealing. This is, to the author's knowledge, the best result ever reported on such a simple n-type process. To further improve this process more investigations have to be done on the origin of the low FF.

References

[1] K. Bothe and J. Schmidt. Electronically activated boron-oxygen-related recombination centers in crystalline silicon. *Journal of Applied Physics*, 2006 ; **99**, 013701.

[2] B.Sopori, P. Basnyat, S. Devayajanam, S. Shet, V. Mehta, J. Binns et al. Understanding Light-Induced Degradation of c-Si Solar Cells. *Proc. 38th IEEE PVSC*. 2010, p. 1115–1120.

[3] D. Macdonald and L.J. Geerligs. Recombination activity of interstitial iron and other transition metal point defects in p- and n-type crystalline silicon. *Appl. Phys. Lett.,* 2004 ; **85**, No. 18,4061–4063.

[4] A.R. Burgers, L.J. Geerligs, A.J. Carr, A. Gutjahr, D.S. Saynova, X. Jingfeng, et al. 19,5% efficient n-type Si solar cells made in production. *Proc. 26th EuPVSEC and Exhibition*, 2011, p. 1144–1147.

[5] N. Bateman, P. Sullivan, C. Reichel, J. Benick, and M. Hermle. *Energy Procedia,* 2011 ; **8**, 509–514.

[6] D.L. Meier, V. Chandrasekaran, H.P. Davis, A.M. Payne, X. Wang, V. Yelundur, et al.. N-Type, Ion-Implanted Silicon Solar Cells andModules. *IEEE Journal of Photovoltaics*, 2011 ; **1**, No. 2,123–129.

[7] J. Benick, N. Bateman and M. Hermle. *Proceedings of the 25th EuPVSEC/WCPEC-5*, 2010, p. 1169–1173.

[8] Y.-W. Ok, A. D. Upadhyaya, Y. Tao, F. Zimbardi, S. Ning, A. Rohatgi, *Proc. 38th IEEE PVSC*, 2012.

[9] H. Boo, J.-H. Lee, M. G. Kang, K.D. Lee, S. Kim, H. C. Hwang, et al. Effect of high-temperature annealing on ion-implanted silicon solar cells. *International Journal of Photoenergy*, 2012 ; Article ID:921908.

[10] A. Lanterne, Y. Veschetti, R. Cabal, S. Gall, D. Ramappa, M. Sheoran, et al. . *Proc. 27th EuPVSEC*, 2012, p. 1897–1900.

[11] D. Pysch, A. Mette, SW Glunz. *Solar Energy Materials & Solar Cells,* 2007 ; **91**, 1698–1706.